J. Chem. Sci. (2019)131:81
https://doi.org/10.1007/s12039-019-1661-2

REGULAR ARTICLE

One-pot synthesis of new water-soluble binuclear octahedral Ni(II) and mononuclear Ru(II) carbonyl complexes containing 2,6 pyridine dicarboxylic acid

P KALAIVANI[a,*], H PUSCHMANN[c], M V KAVERI[b], T SURESH[b] and R PRABHAKARAN[b,*]

[a]Department of Chemistry, Nirmala College for Women, Bharathiar University, Coimbatore, Tamilnadu 641018, India
[b]Department of Chemistry, Bharathiar University, Coimbatore, Tamilnadu 641 046, India
[c]Department of Chemistry, Durham University, Durham DH1 3LE, UK
E-mail: kalaivani19@gmail.com; rpnchemist@gmail.com

MS received 4 December 2018; revised 25 June 2019; accepted 25 June 2019

Abstract. An attempt to synthesize mixed geometrical hetero binuclear complexes has been made by reacting 2,6 pyridinedicarboxylic acid with $[NiCl_2(PPh_3)_2]$ and $[RuHCl(CO)(PPh_3)_3]$. However, the reaction afforded a mononuclear complex $[Ru(dipic)(CO)(PPh_3)_2].DMF$ (**1**) and homo binuclear complex $[Ni_2(dipic)_2(H_2O)_5].2H_2O$ (**2**) [dipic = 2,6-pyridinedicarboxylate] respectively. The new complexes (**1** and **2**) were characterized by elemental analyses, IR, UV-Vis, ^{1}H-NMR and single-crystal X-ray diffraction studies. The complexes **1** and **2** crystallized in the monoclinic $P2_1/c$ and triclinic *P*-1 space groups, respectively. Complex **2** displayed a three-dimensional (*3D*) network with lattice water molecules. The redox behaviour of the complexes was studied by cyclic voltammetry. The DNA and albumin binding studies of the complexes were done by taking CT-DNA and BSA as models. The new complexes exhibited significant binding efficiency with DNA and albumin.

Keywords. Ruthenium(II) complex; binuclear Ni(II) complex; pyridine dicarboxylic acid; NMR; X-ray crystallography; cyclic voltammetry; CT-DNA; BSA.

1. Introduction

In the past decades, the constructions of binuclear centers containing transition metals are ubiquitous in metalloproteins.[1] A number of representative examples of structurally characterized homo- and hetero binuclear active sites[2–7] having asymmetric ligand environments have been reported.[8] Numerous metal complexes are known to accelerate the drug action and the efficacy of the organic therapeutic agent. The efficiency of the different therapeutic agents can be often enhanced[9] upon binding with a suitable metal ion. In addition, the biological activity of metal complexes also primarily depends on the donor atoms of the ligands since different ligands exhibit different biological properties.[10] Among the dicarboxylic acids, pyridine-2,6-dicarboxylic acid is a well-known N,O chelator act as a bidentate, tridentate, meridian and bridging ligand forming stable complexes with metal ions and it has gained more importance in coordination chemistry not only because of their variable binding mode,[11, 12] but also due to its low toxicity and amphiphilic in nature.[13] In addition, they also have shown a wide range of applications in the fields of organic and pharmaceuticals as catalyst, medicines, intermediates, antitumor agent, bactericidal compositions, and insulin-mimetic reagents.[14–16] These observations set an objective to design and synthesize hetero binuclear complexes containing pyridine-2,6-dicarboxylic acid bridged Ni/Ru complexes and study their efficacy in organic synthesis and biology. However, our reaction ended with a mononuclear Ru(II)

*For correspondence

Electronic supplementary material: The online version of this article (https://doi.org/10.1007/s12039-019-1661-2) contains supplementary material, which is available to authorized users.

Published online: 27 August 2019

carbonyl and binuclear Ni(II) complexes instead of the more expected hetero binuclear complex. Herein, we discuss the synthesis, spectral and structural characterization, redox behaviour, DNA/protein binding studies of new mononuclear ruthenium and binuclear nickel(II) complexes from a single pot.

2. Experimental

2.1 *Materials*

All chemicals were reagent grade and were used as received from commercial suppliers unless otherwise stated. All the solvents were dried according to the standard procedures.[17] Commercially available $RuCl_3.3H_2O$ (Himedia) was used without further purification. The starting complexes $[RuHCl(CO)(PPh_3)_3]$,[18] $[NiCl_2(PPh_3)_2]$[19] were prepared as reported earlier. The ligand pyridine 2,6 dicarboxylic acid was purchased from Sigma Aldrich. Melting points were determined with Lab India instrument. Elemental analyses (C, H, N) were performed on Vario EL III Elementar elemental analyzer. Nicolet Avatar Model FT-IR spectrophotometer was used to record the IR spectra (4000–400 cm^{-1}) of the free ligand and the complexes. Electronic absorption spectra were recorded using JASCO 6600 spectrophotometer. ^1H NMR spectra were recorded on Bruker AMX 500 at 500 MHz using tetramethylsilane as an internal standard. The cyclic voltammetric study was carried out on CH instruments Electrochemical Analyzer in DMF using a platinum working electrode and all the potentials were referenced to a saturated Ag/AgCl electrode.

2.2 *Synthesis of complexes*

The ligand 2,6-pyridinedicarboxylic acid (0.27 g, 0.1529 mmol) was dissolved in benzene (20 cm^3) and it was slowly added to $[NiCl_2(PPh_3)_2]$ (0.100 g, 0.1529 mmol) in benzene (20 cm^3) resulted in a green colour solution and to this, $[RuHCl(CO)(PPh_3)_3]$ (0.146 g, 0.1529 mmol) was added and further refluxed for 5 h. A clear yellowish-orange reaction mixture obtained was filtered and allowed to stand at room temperature for 3 days in which it gave yellow precipitate (**1**) and light green crystals of (**2**). Crystals of complex **2** were isolated by handpicking method. The remaining yellow precipitate was checked with TLC and recrystallized from DMF to yield light orange crystals (**1**) which were filtered, washed with n-hexane and dried. $[Ru(dipic)(CO)(PPh_3)_2].(CH_3)_2NCHO$ (**1**): Yield 43%; M.p. 167 °C; Elemental analyses calcd. (%) for $C_{47}H_{40}N_2O_6P_2Ru$: C, 63.29; H, 4.52; N, 3.14%. Found: C, 63.27; H,4.51; N, 3.12%; FT-IR (KBr disks, cm^{-1}) 1663 $\nu_{as}(COO^-)$, 1322 $\nu_s(COO^-)$, 1480(C-O), 1957 (C≡O);

^1H NMR(DMSO-d6, ppm): δ 7.21–7.87 ppm (m, aromatic) corresponding to the protons of triphenylphosphine, amide proton of DMF and the pyridine ring [H3,H4 and H5]; δ 2.5–2.7 (m, methyl group of DMF). UV-visible: λ_{max} (solvent: DMSO)/nm 261 (ε/dm^3 mol^{-1} cm^{-1} 15,358). $[Ni_2(dipic)_2(H_2O)_5].2H_2O$ (**2**) Yield 36%; M.p. 143 °C; Elemental analysis calcd. (%) for $C_{14}H_{20}N_2Ni_2O_{15}$: C, 29.30; H, 3.51; N, 4.88%. Found: C, 29.28; H,3.49; N, 4.87%; FT-IR (KBr disks, cm^{-1}) 1616 $\nu_{as}(COO^-)$, 1384 $\nu_s(COO^-)$, 3484 $\nu(H_2O)$; ^1H NMR (DMSO-d6, ppm): peaks were not found ^1H NMR inactive; UV-visible: λ_{max} (solvent: DMSO)/nm 260 (ε/dm^3 mol^{-1} cm^{-1} 16,427) and 267(ε/dm^3 mol^{-1} cm^{-1} 12,236).

2.3 *X-ray crystallography*

Single light orange irregular-shaped crystals of **1** were recrystallized from DMF by slow evaporation. A suitable crystal (0.58 × 0.33 × 0.18 mm^3) was selected and mounted on a MITIGEN holder in perfluoro ether oil on an Xcalibur, Sapphire3 diffractometer. The crystal was kept at T = 120(2)K during data collection. Using Olex[2, 20] the structure was solved with the Superflip[21] structure solution program, using the Charge Flipping solution method. The model was refined with the SHELXL-97[22] refinement package using Least Squares minimization.

Single light green cube-shaped crystals of **2** were recrystallized from water by slow evaporation. A suitable crystal (0.12 × 0.11 × 0.10 mm^3) was selected and mounted on a hair in perfluoro ether oil on an Xcalibur, Sapphire3 diffractometer. The crystal was kept at T = 293(2)K during data collection. Using Olex[2, 20] the structure was solved with the ShelXS[22] structure solution program, using the Direct Methods solution. The model was refined with SHELXL-97[22] using Least Squares minimization.

2.4 *Binding studies*

2.4a *DNA binding study*: The binding ability of complexes **1** and **2** with CT DNA were carried out in deionised water with tris(hydroxymethyl)-aminomethane (Tris, 5 mM) and sodium chloride (50 mM) and adjusted to pH 7.2 with hydrochloric acid at room temperature. Various concentrations of CT-DNA (0–40 μM) were added to the complexes (10 μM). Absorption spectra were recorded after equilibrium at 20 °C for 10 min. The intrinsic binding constant K_b was determined by using Stern Volmer equation (1).[23, 24]

$$[DNA]/[\varepsilon_a - \varepsilon_f]) = [DNA]/[\varepsilon_b - \varepsilon_f] + 1/Kb[\varepsilon_b - \varepsilon_f] \quad (1)$$

The absorption coefficients ε_a, ε_f, and ε_b correspond to A_{obsd}/[compound], the extinction coefficient for the compound free in solution and the extinction coefficient for the compound in the fully bound form, respectively. The slope and the intercept of the linear fit of the plot of $[DNA]/[\varepsilon_a - \varepsilon_f]$ versus [DNA] give $1/[\varepsilon_a - \varepsilon_f]$ and $1/K_b[\varepsilon_b - \varepsilon_f]$, respectively. The intrinsic binding constant K_b can be obtained from the ratio of the slope to the intercept. It can

be determined by monitoring the changes in the absorbance in the intra ligand band (IL band) at the corresponding λ_{max} with increasing concentration of DNA and is given by the ratio of the slope to the Y-intercept in plots of [DNA]/($\varepsilon_a - \varepsilon_f$) versus [DNA].

2.4b *Competitive binding with ethidium bromide (EB)*: To find out the exact mode of attachment of CT DNA to the fluorescence of the compound quenching, experiments of EB-DNA were carried out by adding 0–30 μM compounds containing 10 μM EB, 10 μM DNA and tris-buffer (pH=7.2). Before measurements, the system was shaken and incubated at room temperature for ~5 min. The emission was recorded at 530–750 nm. The quenching extents of complexes were evaluated qualitatively by employing the Stern–Volmer equation (2).

$$I_0/I = K_{sv}[Q] + 1 \quad (2)$$

where I_o is the emission intensity in the absence of compound, I is the emission intensity in the presence of compound, K_{sv} is the quenching constant, and [Q] is the concentration of the compound. The K_{sv} values have been obtained as a slope from the plot of I_0/I vs [Q].

2.4c *Bovine serum albumin binding study*: Quenching of the tryptophan residues of BSA was performed using complexes as quenchers. To the solutions of BSA (10 μM) in phosphate buffer at pH7, increments of the quenchers were added, and the emission intensity at 341 nm (excitation wavelength at 266 nm) was monitored after each addition of the quencher. The Stern Volmer equation (3) was used to interpret the quenching mechanism and the ratio of the fluorescence intensity in the absence of (I_0) and in the presence of (I_{corr}- corrected fluorescence intensity) the quencher is related to the concentration of the quencher [Q] by a coefficient Ksv.

$$I_0/I_{corr} = 1 + K_{SV}[Q] \quad (3)$$

In order to correct the inner filter effect the following equation 4, is used.

$$\mathbf{I}_{corr} = \mathbf{I}_{obs} * \mathbf{10}\ \frac{Aexc + Aem}{2} \quad (4)$$

where I_{corr} is the corrected fluorescence value, I_{obs} the measured fluorescence value, A_{exc} the absorption value at the excitation wavelength, and A_{em} the absorption value at the emission wavelength.[25]

The binding constant (K_b) and the number of binding sites (n) can be determined according to the Scatchard equation (5).[26]

$$\log[(I_0 - I)/I] = \log K_b + n \log[Q] \quad (5)$$

where, in the present case, K_b is the binding constant for the quencher–fluorophore interaction and n is the number of binding sites per albumin molecule, which can be determined by the slope and the intercept of the double logarithm regression curve of log [(I_0−I)/I] versus log[Q]. Synchronous fluorescence spectra of BSA with various concentrations of complexes (0–25 μM) were obtained from 300 to 500 nm when Δλ = 60 nm and from 290 to 500 nm when Δλ = 15 nm. The excitation and emission slit widths were 5 and 6 nm, respectively. Fluorescence and synchronous measurements were performed by using a 1 cm quartz cell on a JASCO FP 6500 spectrofluorometer.

3. Results and Discussion

The stoichiometric reaction of pyridine 2,6 dicarboxylic acid (0.27 g, 0.1529 mmol) with [$NiCl_2(PPh_3)_2$] and [$RuHCl(CO)(PPh_3)_3$] in benzene (20 cm^3) resulted in two products **1** and **2** (Scheme 1). The suitable crystals of complex **1** and **2** were obtained and characterized by analytical, spectral and X-ray crystallographic methods.

3.1 *Infrared spectroscopy*

The IR spectra of the complexes and the ligand were recorded as KBR pellets and gave preliminary information about the coordination of the ligand to metals. The IR spectrum of the free ligand (H_2dipic) showed predominant vibrations associated with O-H are 2913 cm^{-1} {ν(O-H)}, 1412 cm^{-1} {δ(OH)} and 924 cm^{-1} {γ(O-H)}.[27–29] In addition, a strong band was observed at 1721 cm^{-1} in the free ligand assignable to ν (C=O) of COOH moiety.[30] However, none of these bands were observed in the new complexes **1** and **2**, indicating the deprotonation and subsequent coordination of both –COOH group through oxygen donor atom with the Ru(II) and Ni(II) ions and the coordination of the pyridine nitrogen is indicated by the redshift of the pyridine ring by 15–20 cm^{-1} in-plane and out of plane deformation vibrations were observed near 630–600 and 430–400.[31, 32] In the complexes **1** and **2**, the presence of $-COO^-$ group is revealed by IR spectra which showed absorption bands at 1663–1616 cm^{-1} and 1322–1384 cm^{-1} corresponding to $\nu_{as}(COO^-)$ and $\nu_s(COO^-)$ vibrations, respectively. In the ruthenium–dipic complex **1**, the characteristic bands are found at 1663 and 1480 cm^{-1}. The former band is assignable to the mode of the C=O bond and the latter band is due to the C-O bond.[33] A sharp band occurred at 1957 cm^{-1} indicating the presence of terminal carbonyl group of the ruthenium precursor.[34] In addition, all the characteristic peaks corresponding to the presence of triphenylphosphine were observed in the usual regions.[35] The IR spectrum of the nickel complex **2** exhibited characteristic bands at ν 870 and

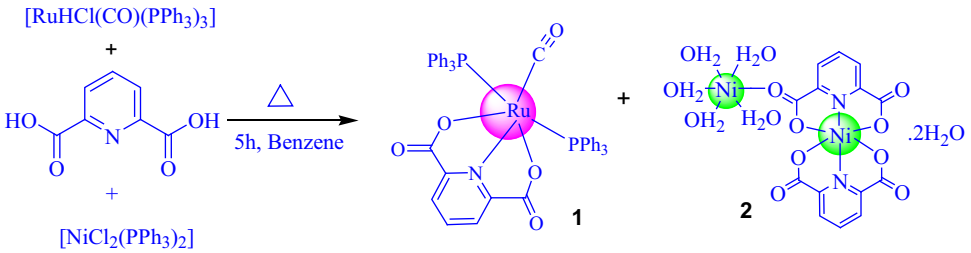

Scheme 1. Preparation of new complexes **1 and 2**.

550 cm^{-1} which are assigned to rocking and wagging modes of the aqua ligands.[36] In addition to $\nu_{as}(COO^-)$ and $\nu_s(COO^-)$ vibrations, the $\nu(H_2O)$ signal is observed at 3484 cm^{-1} for the aqua compound **2**.

3.2 *Electronic Spectroscopy*

The UV visible spectra of the complexes were recorded in methanol in the range of 200–800 nm. The UV-Vis spectra showed peaks at 261 nm (**1**), 260 nm (**2**) and 267 nm (**2**) which are assigned to the ligand centered *n*-π* transition.

3.3 *^{1}H-NMR spectroscopy*

The ^{1}H-NMR spectra of the complexes were taken in DMSO (Figure 1 and S1, Supplementary Information). The spectrum of [H_2dipic)] showed a singlet at δ 11.5 ppm corresponding to -COOH group and this signal completely disappeared in the complex **1** confirming the involvement of phenolic oxygen in coordination. In addition, a broad multiplet was observed in the range 7.21 to 7.87 ppm due to the protons of triphenylphosphine, and the pyridine ring [H3, H4 and H5] suggest the coordination of dipicolinic acid to Ru(II) center. Further, the signal corresponding to the amide proton of lattice DMF also merged with the aromatic region. In addition, two singlets appeared at δ 2.49 and 2.48 ppm corresponding to two non-equivalent methyl groups of N,N dimethylformamide. Complex **2** didn't show any ^{1}H-NMR signals (Figure S1, Supplementary Information).

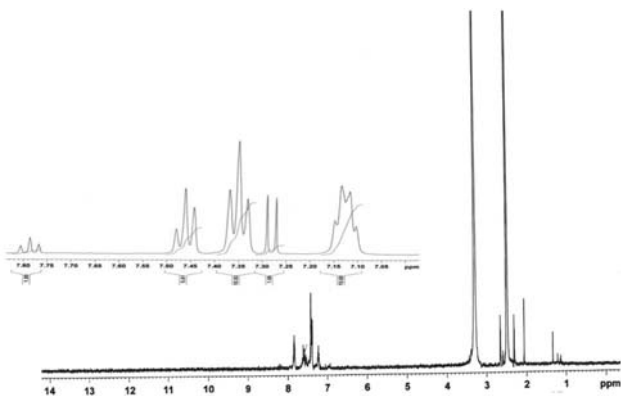

Figure 1. ^{1}H-NMR spectrum of **1**.

3.4 *Description of the crystal structures*

Structures of complexes **1** and **2** have been established by X-ray crystallography revealing that complex **1** is mononuclear ruthenium(II) and **2** is binuclear nickel(II) 2,6 pyridine dicarboxylate (Table 1). The structures of the new complexes are illustrated in Figures 2 and 3, respectively. Ruthenium-dipic complex **1** was crystallized with one unit of DMF in its crystal lattice. In the complex **1**, the bis-deprotonated dipic^{2-} ligand coordinated with the ruthenium center in a tridentate chelating manner through its pyridyl nitrogen atom and two oxygen atoms from both carboxylate groups, the (κ^3-dipic)Ru fragment has an almost planar $RuNO_2$ core structure. The coordination geometry around the Ru(II) is distorted octahedral and is mainly due to the variation in the bond lengths and angles of {RuNO2P2(CO)} core (Table 2). The equatorial sites of the complex are occupied by one nitrogen, two oxygen atoms from the tridentate chelating κ^3-dipic ligand and one terminal carbonyl group. Further, two phosphorous atoms from the triphenylphosphine groups fill up the two axial positions. Usually, triphenylphosphine prefers to take up mutually *cis* positions for better π-interaction,[37] whereas in this complex the presence of CO, a stronger π -acidic ligand, may force the bulky triphenylphosphine to take up *trans* positions for steric reasons. The two Ru-O bond lengths [Ru-O2 2.1008(12), Ru-O3 2.1262(12)] are significantly longer than the Ru-N1 bond length [2.0288(14)] and the localization of single and double C-O bond character are apparent in the two carboxylate fragments in each of κ^3-dipic^{2-} ligand. This ligand coordinated equatorially to the ruthenium atoms

Table 1. Crystallographic data of new Ru(II) and Ni(II) complexes.

	[Ru(dipic)(CO)(PPh_3)$_2$]. $(CH_3)_2NCHO$ (**1**)	[Ni_2(dipic)$_2$(H_2O)$_5$].2H_2O (**2**)
Empirical formula	$C_{47}H_{40}N_2O_6P_2Ru$	$C_{14}H_{20}N_2Ni_2O_{15}$
CCDC	987978	1510043
Formula weight	891.82	573.74
Temperature	120(2)K	293(2)K
Wavelength	0.71073 Å	0.71073 Å
Crystal system	triclinic	monoclinic
Space group	*P*-1	*P*21/*c*
Unit cell dimensions		
a	11.8053(4) Å	8.30994(18) Å
b	13.7140(5) Å	27.0603(6) Å
c	14.3728(4) Å	9.64992(17) Å
Alpha	91.041(3)°	90.00°
Beta	102.986(3)°	98.5680(18)°
Gamma	114.054(3)°	90.00°
Volume	2054.70(13) $Å^3$	2145.75(7) $Å^3$
Z	2	4
Density (calculated)	1.441 Mg/m^3	1.776 Mg/m^3
Absorption coefficient	0.512 mm^{-1}	1.834 mm^{-1}
F(000)	916	1176.0
Theta range for data collection	1.6950 to 30.2520°	2.26 to 30.50°
Index ranges	−15<=h<=15, −17<=k<=17, −18<=l<=18	−11<=h<=11, −38<=k<=38, −13<=l<=13
Reflections collected/unique	42468/9447 [R(int) = 0.0427]	39527/6546 [R(int) = 0.0507]
Completeness to theta	30.2520°	30.50°
Refinement method	Full-matrix least-squares on F^2	Full-matrix least-squares on F^2
Data/restraints/parameters	9447/0/525	6546/0/309
Goodness-of-fit on F^2	1.037	1.185
Final R indices [I> 2sigma(I)]	R1= 0.0270, wR2 = 0.0609	R1= 0.0453, wR2 = 0.0961
R indices (all data)	R1= 0.0327, wR2 = 0.0644	R1= 0.0528, wR2 = 0.0991
Largest diff. peak and hole	0.435 and −0.688 $e.A^{-3}$	1.145 and −0.646 $e.A^{-3}$

with the bite angles of 77.15(5) and 77.80(6) [O3-Ru-N1 and O2-Ru-N1], and the O2–Ru–O3 bond angle is 154.93(5). The average Ru-O bond length is 2.1135(12) Å and the two Ru-P bond lengths are 2.3800(4) and 2.3645(4) Å [Ru-P1and Ru-P2], and the P1-Ru-P2 bond angle is 173.14(2). This shows that the two triphenylphosphine groups are mutually *trans* to each other occupying the axial positions. The Ru–C(carbonyl) bond length is 1.8640(18) Å [Ru-C1]. The bond lengths discussed above are similar and are comparable to those reported Ru(II) carbonyl complexes having triphenylphosphine.[38–42]

Complex **2** formed as an asymmetric unit which is composed of a neutral binuclear motif, five coordinated water molecules, and two free water molecules. In this complex, two nickel atoms are hexa coordinated, and the $dipic^{2-}$ ligand acted as a bridging and a chelating ligand. The resulting coordination compound showed distorted octahedral geometries, as shown in Figure 3. In the first unit, Ni1 is coordinated with four carboxylate oxygen atoms and two pyridine nitrogen atoms from the two $dipic^{2-}$ ligands, with normal Ni–O (2.1046(17) –2.1760(17)Å) and Ni–N (1.970(2) and 1.962(2) Å) bond lengths which lie within the previously reported values of similar complex {[Ni(dipic)$_2$Ni(H_2O)$_5$].2H_2O}.[43]

The two tridentate $dipic^{2-}$ units are almost perpendicular to each other as the bond angles of all O-Ni-O' are significantly varied from 90°, i.e., 86:56(7) ° for {O1B Ni1 O1A}, 93:37(7)° {O2B Ni1 O2A}, 95:25(7) ° {O2B Ni1 O1A}, and 95:35(7)° {O1B Ni1 O2A} and also the bond angle of N1B Ni1 N1A is 174.74(8)° which is deviated from 180̊. From the bond angles, it can be inferred that the nitrogen atoms, N1A and N1B, are placed in the axial positions and the four oxygen atoms, O1A, O1B, O2A and O2B, are occupying the equatorial positions in the distorted octahedral complex (Figure 3). In the second unit, Ni2 is coordinated with six oxygen atoms from five coordinated water molecules and one bridge bidentate carboxylate group (O4A) from one $dipic^{2-}$ ligand with normal Ni–O distance (2.0360(16)Å) resulting in a distorted octahedral environment with *trans* oxygen atoms. The oxygen atom of bidentate carboxylate group (O4A) is *trans* to oxygen atom of second water molecule [O4A- Ni2-O2W 172.42(7)°] and oxygen atoms of remaining four water

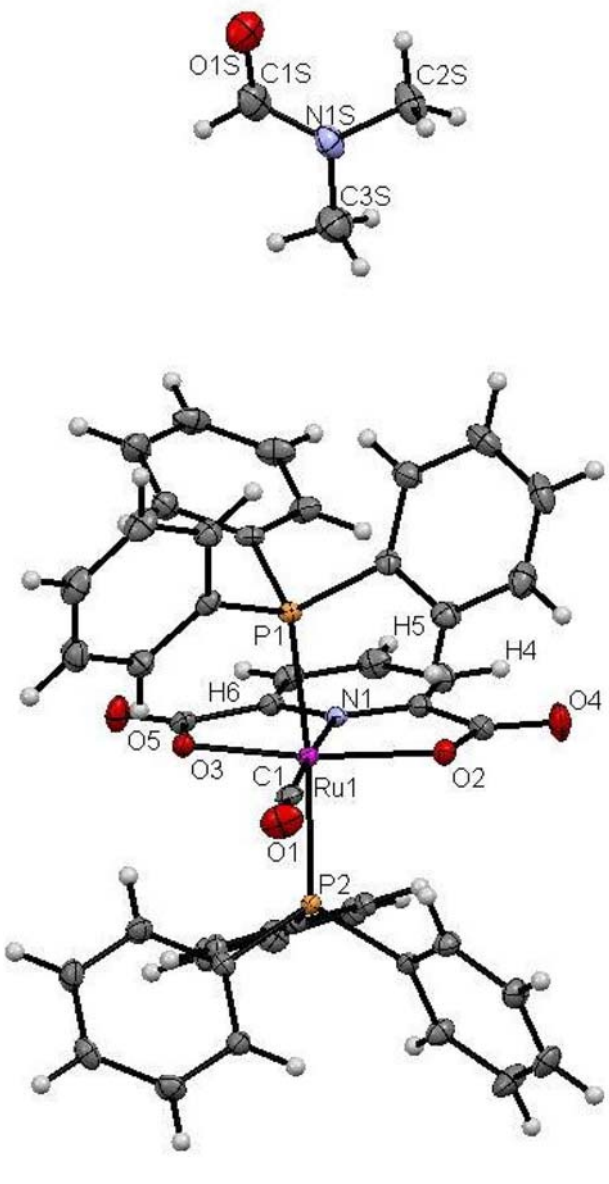

Figure 2. ORTEP diagram of **1**, (Thermal ellipsoids are shown at 50% probability).

molecules are *trans* to each other [O4W-Ni2-O1W 172.37(7)°; O5W-Ni2-O3W 177.17(7)°] (Figures S2 and S3, Supplementary Information). Both the units are further connected by hydrogen bonding through the water molecules, resulting in a *3D* network (Figure S4, Supplementary Information). The hydrogen-bonding parameters are reported in Table S1 (Supplementary Information). In this complex, the lattice water played a vital role in the formation of the *3D* structure.

3.5 *Cyclic voltammetry*

The redox behaviour of new mononuclear ruthenium(II) (**1**) complex and binuclear Ni(II) complex (**2**)

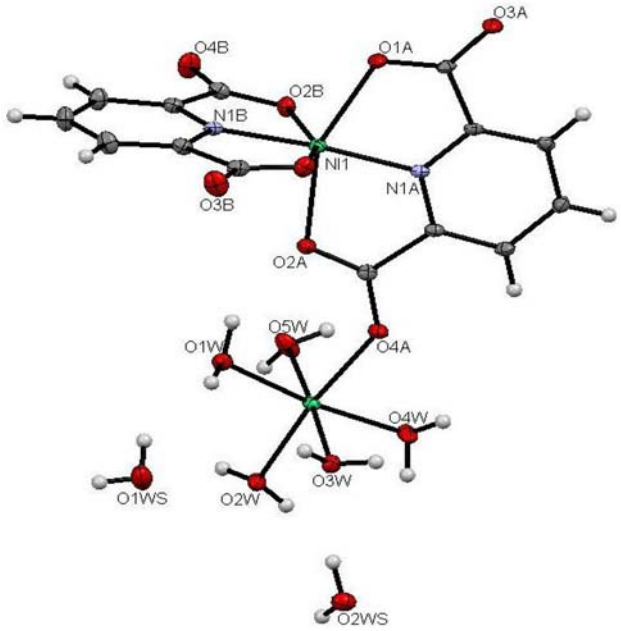

Figure 3. ORTEP diagram of complex **2** (Thermal ellipsoids are shown at 50% probability).

was studied in DMF by using cyclic voltammetry at 100 mV scan rate by using a platinum disc counter electrode and a platinum wire working electrode. All the potentials were referenced to Ag/AgCl electrode. Ferrocene was used as an external standard. Ru(II) complex exhibited a pair of redox waves on both the positive and the negative potential sides, corresponding to one electron quasi-reversible oxidation [Ru(II)-Ru(III)] with the potential of 0.454 V with the peak to peak separation of 272 mV, and one electron quasi-reversible reduction [Ru(II)-Ru(I)] with the potential of −0.90 V with the peak to peak separation of 325 mV (Figure 4a and 4b). Further, quasi-reversible ligand oxidation was seen at 1.17 V with the peak to peak separation of 240 mV. However, the binuclear nickel(II) complex exhibited a reversible one-electron oxidation corresponding to [Ni(II)-Ni(III)] with the potential of 0.060 V with the peak to peak separation of 50 mV. A quasi-reversible ligand reduction with the potential of −1.1 V with the peak to peak separation of 200 mV was observed in the negative potential side. Whereas, an irreversible reduction [Ni(II)-Ni(I)] at 0.25 V and irreversible ligand oxidation at 1.3 V were also observed in the cyclic voltammogram of the complex.

3.6 *DNA-binding studies*

3.6a *UV absorption spectrometry*: Experiments were carried out to check the stability of the

Table 2. Selected bond lengths (Å) and angles (°) of new complexes **1** and **2**.

[Ru(dipic)(CO)(PPh_3)$_2$]. $(CH_3)_2NCHO$ (**1**)	$[Ni_2(dipic)_2(H_2O)_5].2H_2O$ (**2**)
Bond lengths (Å)	Bond lengths (Å)
Ru P1 2.3800(4)	Ni1 O1A 2.1629(17)
Ru O3 2.1262(12)	Ni1 O1B 2.1046(17)
Ru P2 2.3645(4)	Ni1 O2A 2.1760(17)
Ru N1 2.0288(14)	Ni1 O2B 2.1574(17)
Ru O2 2.1008(12)	Ni1 N1A 1.970(2)
Ru C1 1.8640(18)	Ni1 N1B 1.962(2)
Bond angles (°)	Ni2 O1W 2.0530(17)
P1 Ru1 P2 173.14(2)	Ni2 O2W 2.0543(17)
P1 Ru1 O2 94.83(4)	Ni2 O3W 2.1217(17)
P1 Ru1 O3 86.99(4)	Ni2 O4A 2.0360(16)
P1 Ru1 N1 92.35(4)	Ni2 O4W 2.0343(18)
P1 Ru1 C1 88.82(6)	Ni2 O5W 2.0492(19)
P2 Ru1 O2 91.08(4)	Bond angles (°)
P2 Ru1 O3 89.14(4)	O1A Ni1 O2A 154.81(6)
P2 Ru1 N1 92.31(4)	O2B Ni1 O1A 95.25(7)
P2 Ru1 C1 86.80(6)	O2B Ni1 O2A 93.37(7)
O2 Ru1 O3 154.93(5)	N1A Ni1 O1A 77.15(7)
O2 Ru1 N1 77.80(6)	N1A Ni1 O1B 102.44(7)
O2 Ru1 C1 99.04(7)	N1A Ni1 O2A 77.91(7)
O3 Ru1 N1 77.15(5)	N1A Ni1 O2B 102.04(7)
O3 Ru1 C1 105.99(7)	N1B Ni1 O1A 108.09(7)
N1 Ru1 C1 176.71(7)	N1B Ni1 O1B 78.52(7)
	N1B Ni1 O2A 96.87(7)
	N1B Ni1 O2B 77.44(7)
	N1B Ni1 N1A 174.74(8)
	O1W Ni2 O2W 95.96(7)
	O1B Ni1 O1A 86.56(7)
	O1W Ni2 O3W 91.99(7)
	O1B Ni1 O2A 95.35(7)
	O2W Ni2 O3W 85.56(7)
	O1B Ni1 O2B 155.23(7)
	O4A Ni2 O1W 91.58(7)
	O4A Ni2 O2W 172.42(7)
	O4A Ni2 O3W 93.40(7)
	O4A Ni2 O5W 88.13(7)
	O4W Ni2 O1W 172.37(7)
	O4W Ni2 O2W 91.60(7)
	O4W Ni2 O3W 89.60(8)
	O4W Ni2 O4A 80.88(7)
	O4W Ni2 O5W 92.99(8)
	O5W Ni2 O1W 85.58(8)
	O5W Ni2 O2W 93.23(8)
	O5W Ni2 O3W 177.17(7)

complexes in tris-HCl (pH-7.2) and it was found that they were stable even after 24 h (Figure S5, Supplementary Information). The binding ability of the complexes to CT-DNA was performed by using UV absorption and fluorescence spectrometry. The absorption spectra of complexes **1** and **2** in the absence and presence of CT-DNA at different concentrations (0–40 μM) are given in Figures 5 and 6. The absorption peaks are 261 nm for complex **1**, 260 and 267 nm for complex **2** which can be attributed to intra-ligand (IL) π–π* transition. As the concentration of CT-DNA increased, complex **1** showed hypochromism with 6 nm red shift at 261 nm. The spectra of complex 2 showed two IL bands of at 260 nm showed hypochromism with 1 nm red shift and at 267 nm with negligible shifts in wavelength. This implies that the two complexes interact with CT-DNA basically through the intercalative mode because intercalation would lead to hypochromism and bathochromism in UV absorption spectra. The intercalative mode involved a strong interaction between the complex and the base pairs of DNA. The binding constant K_b

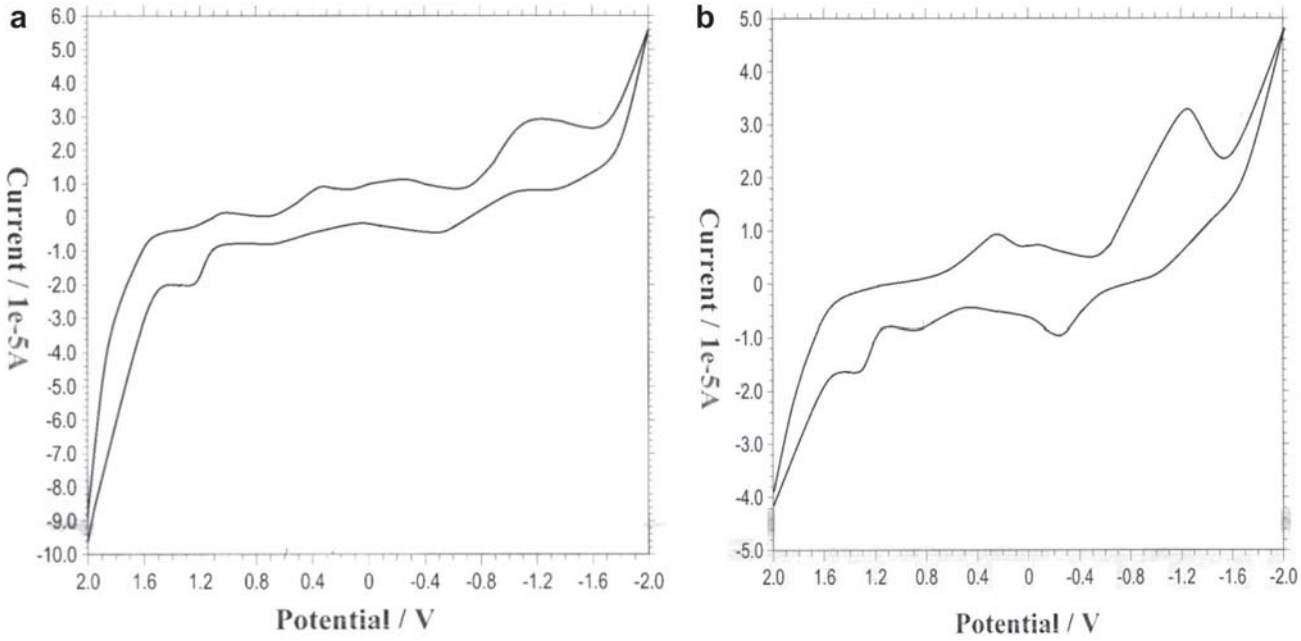

Figure 4. (a) Cyclic voltammogram of **1.** (b) Cyclic voltammogram of **2**.

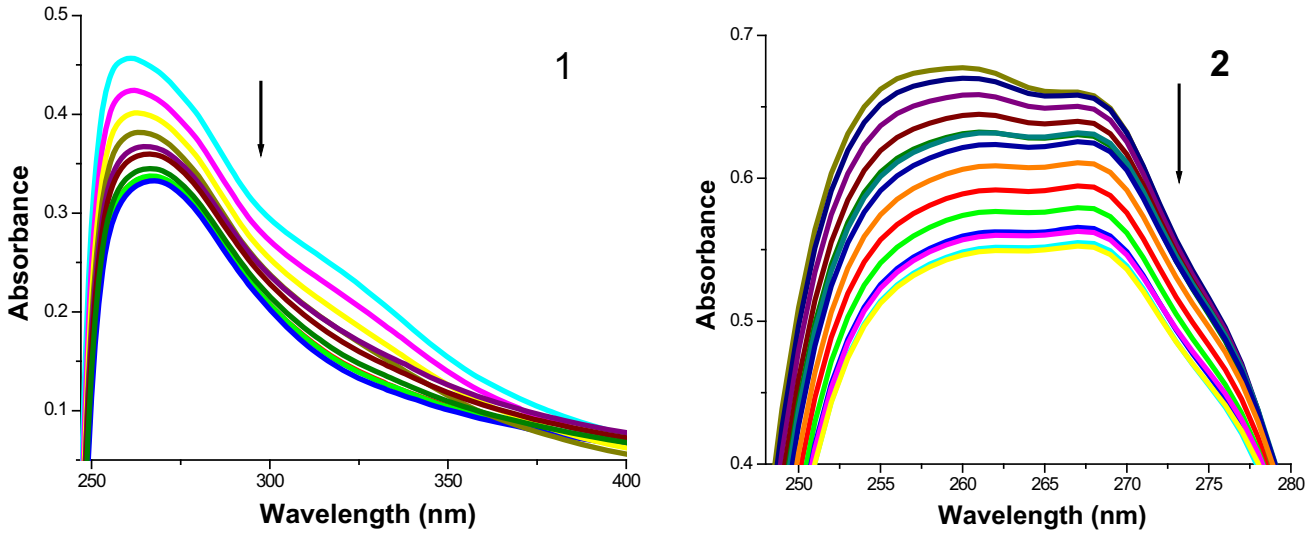

Figure 5. Absorption titration spectra of **1** and **2** with increasing concentrations (0–40 μM) of CT-DNA (tris HCl buffer, pH 7.2).

was determined using the equation.[44] The intrinsic binding constants K_b is 9.04 $\times 10^5$ M^{-1} for **1** and 9.07 $\times 10^4$ M^{-1} for **2** suggesting that the complexes were bound to DNA in an intercalative mode.

3.6b *Competitive binding between EB and complexes for CT DNA*: The competitive EB binding studies may be carried out in order to examine the binding of each complex with CT-DNA. The fluorescence intensity of EB-DNA could be decreased by addition of the complexes as quenchers, indicating the competition between the complexes and EB in binding to DNA that proved the intercalation of metal complexes to the base pairs of DNA.[44, 45] The emission spectra of EB bound to DNA in the absence and presence of the new complexes **1** and **2** are shown in Figure 7. From the figure, it is clear that an appreciable reduction in the fluorescence intensities with negligible wavelength shift was observed on addition of Ru(II) complexes and Ni(II) dicarboxylate complexes to DNA pre-treated with EB, indicating the replacement of EB molecules accompanied by the intercalation of the complexes with DNA. The quenching of EB bound to DNA by the new

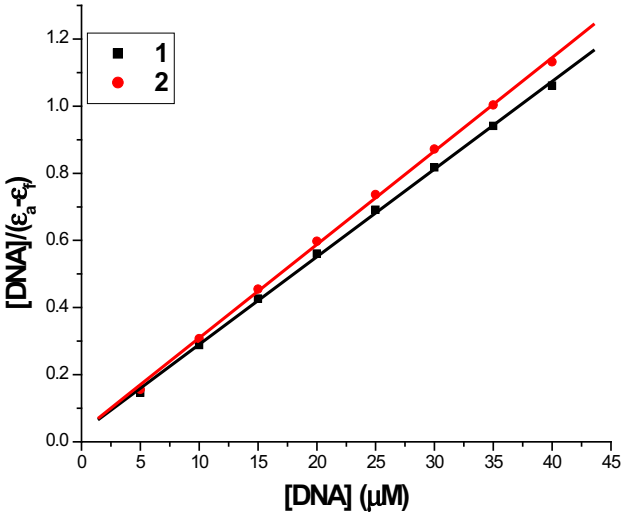

Figure 6. Plot of I_0/I vs log[Q].

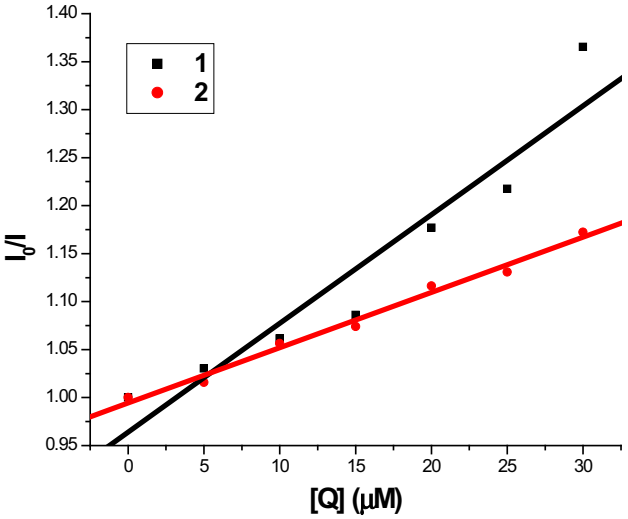

Figure 8. Stern–Volmer plot.

complexes are in good agreement with the linear Stern-Volmer equation (Figure 8). The ratio of the slope to the intercept obtained by plotting I_0/I vs [Q] yielded the quenching constant (Kq) value for complexes **1** and **2** as 1.13×10^4 M^{-1} and 5.76×10^3 M^{-1} respectively.

3.6c *Interaction of complexes 1 and 2 with Bovine Serum Albumin*: Bovine serum albumin (BSA) is the most extensively studied serum albumin, due to its structural homology with human serum albumin (HSA). It binds a variety of substrates including metal cations, hormones, and most therapeutic drugs. The UV absorption spectrum is useful to distinguish the type of quenching exist i.e., static or dynamic quenching and also explores the structural change and the complex formation in solution.[46] The UV absorption spectra of BSA in the presence and absence of new complexes (Figure 9) showed that the absorption intensity of BSA was enhanced with the addition of these complexes from 246 to 253 nm. There was a redshift of 3 nm and 7 nm for the complex–BSA spectrum of **1** and 2. This phenomenon indicates the interaction of BSA with the complexes.[47] The formation of a non-fluorescence ground-state complex induced the change in the absorption spectrum of fluorophore. Thus, possible quenching mechanism of BSA by **1** and **2** was a static quenching

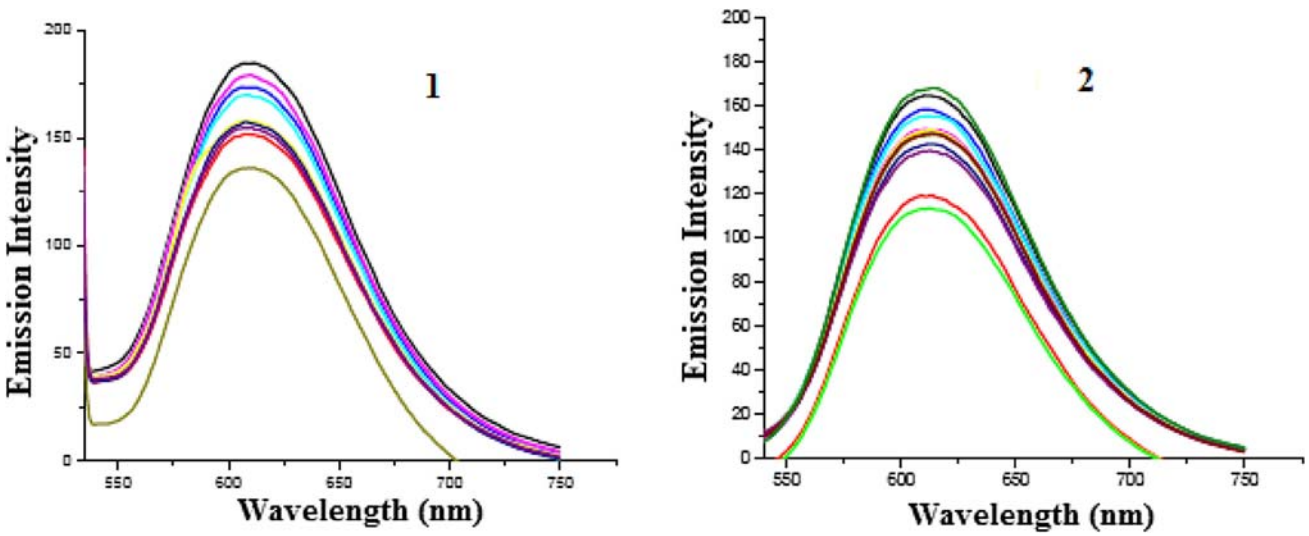

Figure 7. The emission spectra of the DNA–EB system (λ_{exc} = 515 nm, λ_{em} = 550–750 nm), in the presence of complexes **1** and **2**. [DNA] = 10 μM, [EB] = 10 μM. The arrow shows the emission intensity changes upon increasing the amount of complex.

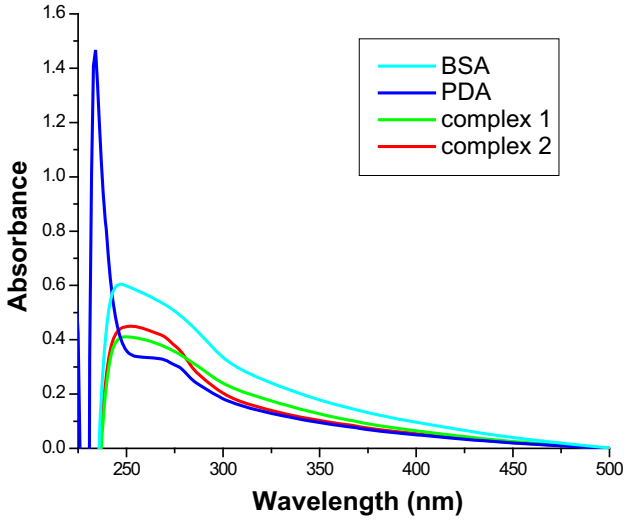

Figure 9. UV absorption spectra of BSA (10 μM) in the absence and presence of compounds (10 μM).

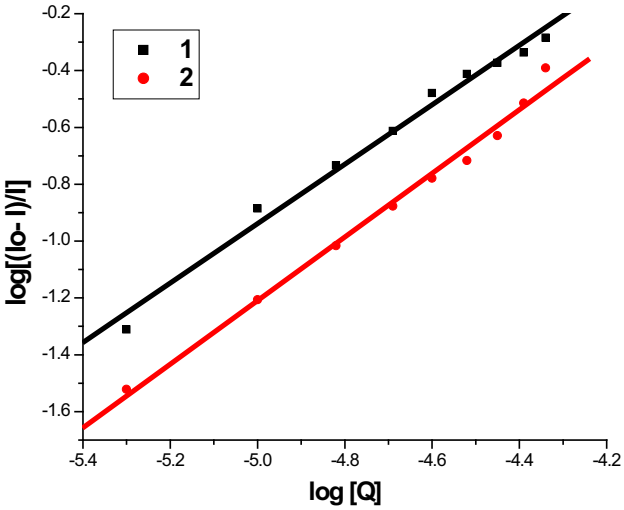

Figure 11. Scatchard plot.

process.[48] The fluorescence spectra of BSA in the presence of increasing amounts of complexes **1** and **2** were recorded in the range 300−450 nm upon excitation of the tryptophan residue at 290 nm (Figure 10). The complexes caused a concentration-dependent quenching of fluorescence without changing the emission maximum or shape of the peaks at 340 and 341 nm as seen in Figure 10. All these data indicate an interaction of the complexes with BSA. The fluorescence data were analyzed by the Stern-Volmer equation. While a linear Stern-Volmer plot is indicative of a single quenching mechanism. The Stern-Volmer quenching constant K_q obtained from the plot of I_0/I vs [Q] was found to be 1.16×10^4 M^{-1} and 8.58×10^3 M^{-1} corresponding to complexes **1** and **2** respectively.

For the static quenching interaction, the binding constant (K_b) and the number of binding sites (n) can be determined according to the method,[49] using the Scatchard equation 5. From the slope and the intercept of the double logarithm regression curve of log $[(I_0-I)/I]$ versus log[Q] (Figure 11) the values of "n" at room temperature are approximately derived to be equal to **1**, which indicates that there is just one single binding site in BSA for the complexes **1** and **2**.

3.6d *Synchronous fluorescence spectroscopic studies of BSA*: Synchronous fluorescence spectra gave the

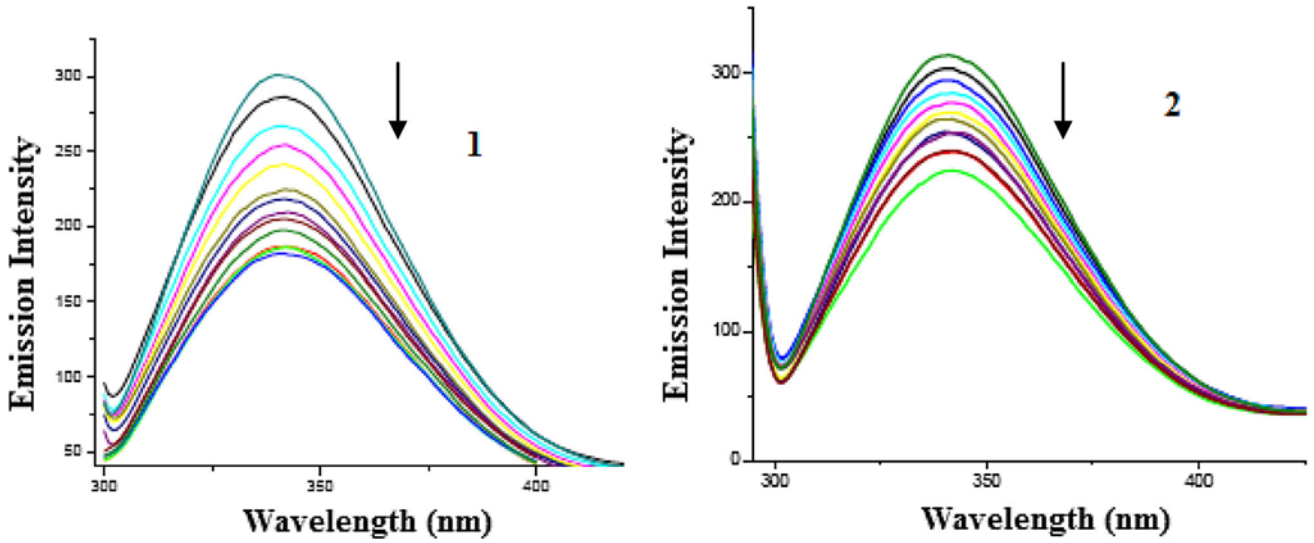

Figure 10. The emission spectrum of BSA (10 μM; λ_{exc} = 280 nm; λ_{emi} = 346 nm) in the presence of increasing amounts of complexes **1** and **2** (0–25 μM). The arrow shows the emission intensity changes upon increasing complex concentration.

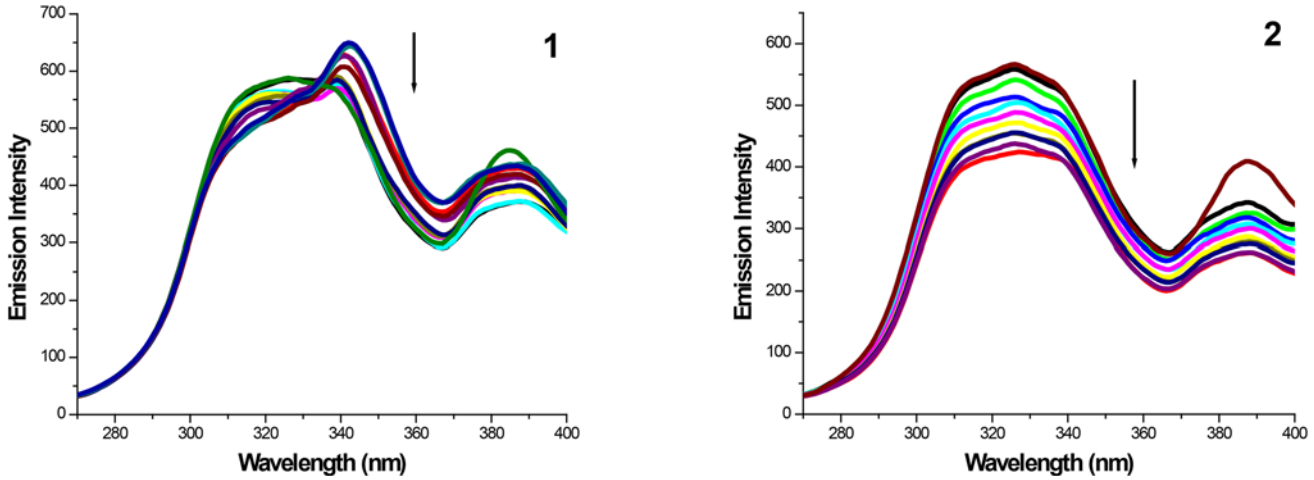

Figure 12. Synchronous spectra of BSA (10 μM) in the presence of increasing amounts of complexes **1**–**4** (0–25 μM) for a wavelength difference of Δλ= 15 nm. The arrow shows the emission intensity changes upon the increasing concentration of complex.

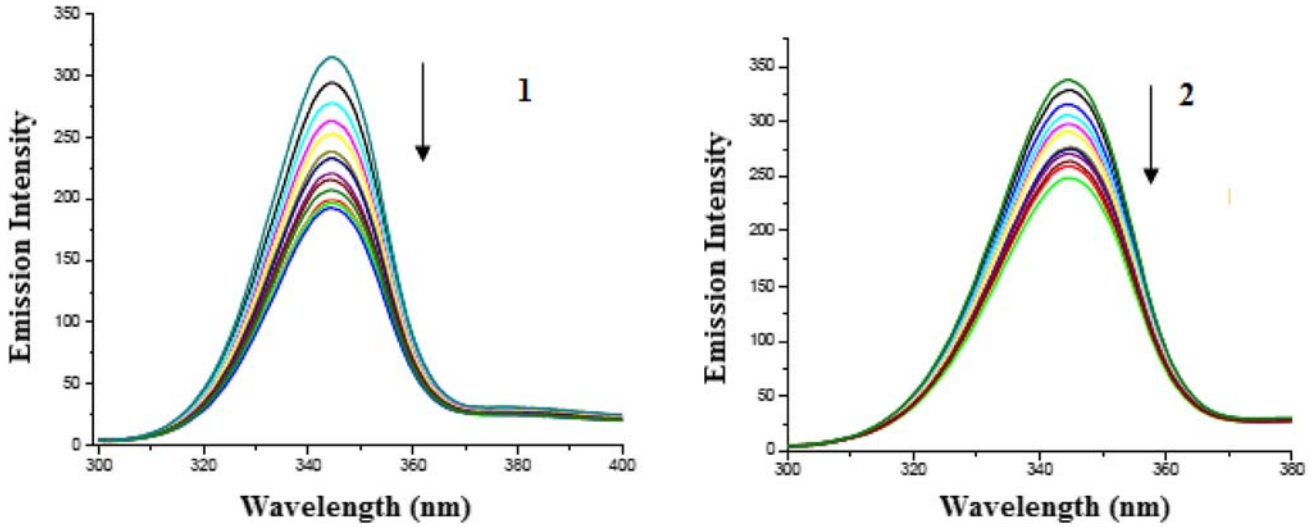

Figure 13. Synchronous spectra of BSA (1 μM) in the presence of increasing amounts of complexes **1** and **2** (0–25 μM) for a wavelength difference of Δλ= 60 nm. The arrow shows the emission intensity changes upon the increasing concentration of complex.

information about the molecular environment in the vicinity of the fluorophore moieties of BSA.[50] When the difference (Δλ) between the excitation and emission wavelengths is fixed at 15 and 60 nm, and the number of complexes (**1** and **2**) added to BSA (10 μM) is increased, a large decrease in fluorescence intensity in the tryptophan emission maximum is observed (Figure 12). In contrast, the emission intensity of tyrosine residue increases in the emission maximum (Figure 13). From the result, we conclude that complexes mainly bind to tryptophan residues of BSA and in the presence of the complexes, the hydrophobicity of microenvironment around tryptophan residues was decreased.

4. Conclusions

Equimolar reaction of 2,6 pyridinedicarboxylic acid with $[NiCl_2(PPh_3)_2]$ and $[RuHCl(CO)(PPh_3)_3]$ resulted in the formation of two structurally different complexes $[Ru(dipic)(CO)(PPh_3)_2].DMF$ (**1**) and $[Ni_2(dipic)_2(H_2O)_5].2H_2O$ (**2**). The complexes have been characterized by various analytical and spectroscopic (IR, UV-Vis, ^{1}H-NMR) techniques. Further, the structure of the complexes was confirmed by single crystal X-ray diffraction studies. The complexes **1** and **2** crystallized in the monoclinic $P2_1/c$ and triclinic $P\,\bar{1}$ space groups respectively. The redox behaviour of the complexes was studied by cyclic voltammetry.

CT-DNA binding studies of the complexes showed their intercalative binding behaviour. BSA binding studies of the complexes revealed their static quenching efficacy.

Supplementary Information (SI)

Crystallographic data for the complexes **1** and **2** have been deposited at the Cambridge Crystallographic centre as supplementary publication (CCDC No. 987978 and CCDC No. 1510043). The data can be obtained free of charge at www.ccdc.cam.ac.uk/conts/retrieving.html/. Table S1 and Figures S1-S5 are available at www.ias.ac.in/chemsci.

Acknowledgement

The author P. K. gratefully acknowledges Department of Science and Technology (DST-SERB), New Delhi, India (No. SB/FT/CS-056-/2014 dated 12.08.2015) for the financial support.

References

1. (a) K D Karlin and Z Tylekar Z (Eds.) 1993 *Bioinorganic Chemistry of Copper* (New York: Chapman & Hall) p. 213; (b) Que L and True A E 1990 Dinuclear Iron- and Manganese-Oxo Sites in Biology *Prog. Inorg. Chem.* **38** 97; (c) Solomon E I, Baldwin M J and Lowery M D 1992 Electronic absorption spectroscopy of proteins: contributions to reactivity *Chem. Rev.* **92** 521
2. Barynin V V, Vagin A A, Melik-Adamyan V R, Grebenko A I, Khangulov S V, Popov A N, Andrionova M E and Vainshtein B K 1986 Metal ions in biological systems *Dokl. Akad. Nauk. SSSR* **288** 887
3. Jabri E, Carr M B, Hausinger R P and Karplus P A 1995 The crystal structure of urease from Klebsiellaaerogenes *Science* **268** 998
4. Kim E E and Wyckoff H W 1991 Reaction mechanism of alkaline phosphatase based on crystal structures: Two-metal ion catalysis *J. Mol. Biol.* **218** 449
5. (a) Tainer J A, Getzoff E D, Beem K M, Richardson, J S and Richardson D C 1982 Determination and analysis of the 2 A-structure of copper, zinc superoxide dismutase *J. Mol. Biol.* **160** 181; (b) Tainer J A, Getzoff E D, Richardson J S and Richardson D C 1983 Structure and mechanism of copper, zinc superoxide dismutase *Nature* **306** 284
6. Strater N, Klabunde T, Tucker P, Witzel V and Krebs B 1995 Crystal structure of a purple acid phosphatase containing a dinuclear Fe(III)-Zn(II) active site *Science* **268** 1489
7. Egloff M P, Cohen P T, Reinemer P and Barford D 1995 Crystal structure of the catalytic subunit of human protein phosphatase 1 and its complex with tungstate *J. Mol. Biol.* **254** 942
8. Belle C and Pierre J L 2003 Asymmetry in Bridged Binuclear Metalloenzymes: Lessons for the Chemist *Eur. J. Inorg. Chem.* 4137
9. Goldstein M, Barton J K, Goldberg J M, Kumar C V and Turro N J 1986 Binding modes and base specificity of tris(phenanthroline)ruthenium(II) enantiomers with nucleic acids: tuning the stereo selectivity *J. Am. Chem. Soc.* **108** 2081
10. Delaney S, Pascaly M, Bhattacharya P K, Han K and Barton J K 2002 Oxidative damage by ruthenium complexes containing the dipyridophenazine ligand or its derivatives: a focus on intercalation *Inorg. Chem.* **41** 1966
11. Grossel M C, Golden C A, Gomm J R, Horton P N, Merckel D A S, Oszer M E and Parker R A 2001 Solid-state behaviour of pyridine-2,6-dicarboxylate esters: supramolecular assembly into infinite tapes *CrystEngComm* **3** 170
12. Ducommun Y, Helm L, Laurenezy G and Merbach A 1989 Variable pressure spectrophotometric equilibrium and ^{139}La NMR kinetic studies of lanthanum(III) ion complex formation with 2,6-dicarboxy-4-hydroxypyridine in aqueous solution *Inorg. Chim. Acta* **158** 3
13. Norkus E and Stalnioniene I 2002 Cu(II), Pb(II) and Cd(II) complex formation with pyridine-2,6-dicarboxylate and 4-hydroxypyridine-2,6-dicarboxylate in aqueous solutions *Chemija (Vilnius)* **13** 194
14. Çolak AT, Çolak F, Yesilel O Z and Büyükgüngör O 2009 Synthesis, spectroscopic, thermal, voltammetric studies and biological activity of crystalline complexes of pyridine-2,6-dicarboxylic acid and 8-hydroxyquinoline *J. Mol. Struct.* **936** 67
15. Kirillova M V, Guedes da Silva M F C, Kirillov A M, Frausto da Silva J J R, Pombeiro A J L 2007 3D hydrogen bonded heteronuclear Co(II), Ni(II), Cu(II) and Zn(II) aqua complexes derived from dipicolinic acid *Inorg. Chim. Acta* **360** 506
16. Moghimi A, Moosavi S M, Kordestani D, Maddah B, Shamsipur M, Aghabozorg H, Ramezanipour F and Kickelbick G 2007 Pyridine-2,6-bis(monothiocarboxylic) acid and 2-aminopyridine as building blocks of a novel proton transfer compound: Solution and X-ray crystal structural studies *J. Mol. Struct.* **828** 38
17. Vogel A I 1989 *Text Book of Practical Organic Chemistry* Vth ed. (London: Longman) p. 268
18. Ahmad N, Levison J J, Robinson S D, Uttley M F, Wonchoba E R and Parshall G W 1974 Complexes of Ruthenium, Osmium, Rhodium, and Iridium Containing Hydride Carbonyl, or Nitrosyl Ligands *Inorg. Synth.* **15** 45
19. Venanzi J 1958 Tetrahedral nickel(II) complexes and the factors determining their formation. Part I. Bis triphenylphosphine nickel(II) compounds *J. Chem. Soc.* **719**
20. Dolomanov O V, Bourhis L J, Gildea R J, Howard J A K and Puschmann H 2009 Olex2: A complete structure solution, refinement and analysis program *J. Appl. Cryst.* **42** 339
21. Palatinus L and Chapuis G 2007 Superflip - A computer program for the solution of crystal structures by charge flipping in arbitrary dimensions *J. Appl. Cryst.* **40** 786

22. Sheldrick G M 2008 A short history of Shelx *Acta Cryst.* **A64** 112
23. Wolfe A, Shimer G H and Meehan T 1987 Polycyclic aromatic hydrocarbons physically intercalate into duplex regions of denatured DNA *Biochemistry* **26** 6392
24. Cohen G and Eisenberg H 1969 Viscosity and sedimentation study of sonicated DNA–proflavine complexes *Biopolymers* **8** 45
25. Van de Weert M and Stella L 2010 Fluorescence Quenching to Study Protein-ligand Binding: Common Error *J. Fluoresc*. **20** 625
26. Jiang M, Xie M X, Zheng D, Liu Y, Li X Y and Chen X 2004 Spectroscopic studies on the interaction of cinnamic acid and its hydroxyl derivatives with human serum albumin *J. Mol. Struct.* **692** 71
27. Carmona P 1980 Vibrational spectra and structure of crystalline dipicolinic acid and calcium dipicolinatetrihydrate *Spectrochim. Acta* **A36** 705
28. Robinson S D and Uttley M F 1973 Complexes of the platinum metals. Part II. Carboxylato(triphenylphosphine) derivatives of ruthenium, osmium, rhodium, and iridium *J. Chem. Soc. Dalton Trans.* 1912
29. González-Baro A C, Pis-Diez R, Piro O E and Parajón-Costa B S 2008 Crystal structures, theoretical calculations, spectroscopic and electrochemical properties of Cr(III) complexes with dipicolinic acid and 1,10-phenantroline *Polyhedron* **27** 502
30. Sengupta P, Ghosh S and Mak T C W 2001 A new route for the synthesis of bis(pyridine dicarboxylato)bis(triphenylphosphine) complexes of ruthenium(II) and X-ray structural characterisation of the biologically active trans-[Ru(PPh3)2(L1H)2] (L1H2= pyridine 2,3-dicarboxylic acid) *Polyhedron* **20** 975
31. Clark R J H and Williams C S 1965 The Far-Infrared Spectra of Metal-Halide Complexes of Pyridine and Related Ligands *Inorg. Chem.* **4** 350
32. Gill N S, Nuttal R H, Scaife D E and Sharp D W A 1961 The infra-red spectra of pyridine complexes and pyridinium salts *J. Inorg. Nucl. Chem.* **18** 79
33. Kamatchi T S, Chitrapriya N, Lee H, Fronczek C F, Fronczek F R and Natarajan K 2012 Ruthenium(II)/(III) complexes of 4-hydroxy-pyridine-2,6-dicarboxylic acid with PPh_3/$AsPh_3$ as co-ligand: Impact of oxidation state and co-ligands on anticancer activity *in vitro Dalton Trans*. **41** 2066
34. Prabhakaran R, Krishnan V, Pasumpon K, Sukanya D, Wendel E, Jayabalakrishnan C, Bertagnolli H and Natarajan K 2006 Preparation, spectral characterization, electrochemistry, EXAFS, antibacterial and catalytic activity of new ruthenium (III) complexes containing ONS donor ligands with triphenylphosphine/arsine *Appl. Organomet. Chem.* **20** 203
35. Archaryya R, Basuli F, Peng S M, Lee G H, Falvello L R and Bhattacharya S 2006 Rhodium Assisted C−H Activation of Benzaldehyde Thiosemicarbazones and Their Oxidation via Activation of Molecular Oxygen *Inorg. Chem.* **45** 1252
36. Nakamoto K 2009 *Infrared and Raman Spectra of Inorganic and CoordinationCompounds* sixth edn. Part B (New York: Wiley) **64** p. 58
37. Basuli F, Peng S M and Bhattacharya S 2001 Chemical Control on the Coordination Mode of Benzaldehyde Semicarbazone Ligands. Synthesis, Structure, and Redox Properties of Ruthenium Complexes *Inorg. Chem.* **40** 1126
38. Srivastava R S and Fronczek F R 2001 Synthesis and crystal structures of carbonyl derivatives of chloride–tetramethylenesulfoxide–ruthenium(III) complexes: $[RuCl_3(TMSO)_2(CO)]$ and $[H(TMSO)_2]$ $[RuCl_4(TMSO)(CO)]$ *Inorg. Chim. Acta* **322** 32
39. Hijazi A, Djukic J P, Pfeffer M, Ricard L, Gruber N K, Raya J, Bertani P and De Cian A 2006 Direct Ortho-ruthenation of Planar Prochiral Pyridine Derivatives by C−H Bond Activation with [Ru(CO)2Cl2]n and Its Unexpected Stereo selectivity *Inorg. Chem.* **45** 4589
40. Chitrapriya N, Mahalingam V, Zeller M and Natarajan K 2008 Synthesis, characterization and crystal structures of cyclometallatedRu(II) carbonyl complexes formed by hydrazones *Polyhedron* **27** 1573
41. Sengupta P, Dinda R, Ghosh S and Sheldrick W S 2001 Synthesis and characterisation of some ruthenium(II) complexes of α-N heterocyclic carboxylic acids- X-ray structures of cis-$[Ru(PPh_3)_2(L^1)_2]$. $2CH_3OH$ and cis-$[Ru(PPh_3)_2(L^3H)_2](L^1H$= pyridine 2-carboxylic acid and L^3H_2=imidazole 4,5-dicarboxylic acid) *Polyhedron* **20** 3349
42. Sengupta P, Ghosh V and Mak T C W 2001 A new route for the synthesis of bis(pyridine dicarboxylato)bis(triphenylphosphine) complexes of ruthenium (II) and X-ray structural characterization of the biologically active *trans*-$[Ru(PPh_3)_2(L^1H_2)]$ (L^1H_2= pyridine 2,3-dicarboxylic acid) *Polyhedron* **20** 975
43. Borah M J, Singh R K B, Sinha U B, Swu T and Borah P J 2012 Synthesis through proton transfer reaction, structure and spectroscopic characterisation of novel anionic nickel (II) complex with pyridine-2,6-dicarboxylic acid and 4-aminobenzenesulfonamide *J. Chem. Crystallogr.* **42** 67
44. Bai G Y, Wang K Z and Duan L H 2004 Luminiscent pH sensing and DNA binding properties of a noel ruthenium (II) complex *J. Inorg. Biochem.* **98** 1017
45. Tysoe S A, Kopelman R and Schelzig D 1999 Flipping the molecular light switch off: Formation of DNA-bound heterobimetallic complexes using $Ru(bpy)_2tpphz^{2+}$ and transition metal ions *Inorg. Chem.* **38** 5196
46. Hu Y J, Liu Y, Wang J B, Xiao X H and Qu S S 2004 Study of the interaction between mono ammonium glycyrrhizinate and bovine serum albumin *J. Pharm. Biomed. Anal.* **36** 915
47. Yue Y Y, Chen X G, Qin J and Yao X J 2008 Investigation of the Interaction between Patulin and Human Serum Albumin by a Spectroscopic Method, Atomic Force Microscopy, and Molecular Modeling *Dye. Pigm.* **79** 176
48. Liu H Y, Xu Z H, Liu X H, Xi P X and Zeng Z Z 2009 Analysis of binding interaction between bovine serum albumin and cobalt (II) complex with salicylaldehyde-2-phenylquinoline-4-carboylhydrazone *Chem. Pharm. Bull*. **57** 1237
49. Jiang M, Xie M. X. Zheng D, Liu Y, Li X Y and Chen X 2004 Spectroscopic studies on the interaction of cinnamic acid and its hydroxyl derivatives with human serum albumin *J. Mol. Struct.* **692** 71
50. Wang N, Ye L, Zhao B Q and Yu J X 2008 Spectroscopic studies on interaction of efonidipine with bovine serum albumin *J. Med. Biol. Res.* **41** 589